Journal of Computational Applied Mechanics 2026, 57(4): 597-614

DOI: 10.22059/jcamech.2026.420974.1929

RESEARCH PAPER

Analytical Solutions for Static Analysis of Sandwich Cylindrical Shell Containing Functionally Graded Face Sheets and Functionally Graded Porosity Core Based on HSDT Theory

Mourad Chitour [a, b, *], Faicel Khadraoui [a], Noureddine Sid [a, b], Abdelhakim Bouhadra [c, d], Abderrahmane Menasria [c, d], Kelifa Mansouri [a,b], Berkia A Elhak [a], Athmani.Moussa [a], Filipe Fernandes [e, f] Abdelouahed Tounsi [g]

[a] *Faculty of Sciences & Technology, Mechanic Eng Department, University Abbes Laghrour, Khenchela 40000, Algeria*

[b] *Laboratory of Eng and Sciences of Advanced Materials (ISMA), Khenchela 40000, Algeria*

[c] *Faculty of Sciences & Technology, Civil Eng Department, University Abbes Laghrour, Khenchela 40000, Algeria*

[d] *Materials and Hydrology Laboratory, University of Sidi Bel Abbes, Faculty of Technology, Civil Engineering Department, Sidi Bel Abbes, 22000 Algeria*

[e] *University of Coimbra, CEMMPRE, ARISE, Department of Mechanical Engineering, Rua Luís Reis Santos, 3030-788, Coimbra, Portugal*

[f] *CIDEM, ISEP, Polytechnic of Porto, Rua Dr. António Bernardino de Almeida, 431, 4249-015 Porto, Portugal*

[g] *Department of Civil and Environmental Engineering, King Fahd University of Petroleum & Minerals, 31261 Dhahran, Eastern Province, Saudi Arabia*

Abstract

In this research, a new four-variable Shear Deformation Theory is utilized to investigate the bending behavior of Imperfect FG sandwich cylindrical shell that are exposed to a load that is distributed evenly. In this theory, the number of unknowns is reduced to four by employing an undefined integral. Furthermore, there is no requirement for any shear correction factor to be included in theory. Furthermore, it is believed that the effective constituent material properties of the top and lower layers of the FG sandwich cylindrical shell fluctuate smoothly and continuously only in the thickness direction. In contrast, the core layer made of porous material. The notion of virtual displacement is utilized to obtain the equations that control equilibrium for simply supported FGSCSs. By applying Navier's method to several different FGSCS schemas, they can derive their respective analytical solutions. A comparison is made between the results obtained and those of previously published research. Within the scope of this investigation, the power law index, side-to-thickness ratio, porosity distribution type and geometric ratio impact on the bending behavior were all taken into consideration.

Keywords: bending behavior, sandwich shells, Property Gradient Materials; Principle of virtual work; Navier's solution.

1. Introduction

Functionally graded materials (FGMs) have attracted increasing interest in advanced engineering applications

* Corresponding author.: *E-mail address:* chitour.mourad@univ-khenchela.dz

owing to the continuous variation of their material properties, which effectively reduces stress concentrations and delamination phenomena typically observed in laminated composites. Owing to their superior thermal resistance, high stiffness-to-weight ratio, and remarkable mechanical performance, FGM sandwich structures have been extensively employed in aerospace, civil, mechanical, and naval engineering applications. Within this class of structures, doubly curved shells play a significant role owing to their high load-carrying capacity and excellent structural efficiency under severe mechanical and thermal loading conditions[1, 2].

The rapid development of functionally graded materials (FGMs) has prompted extensive research aimed at characterizing their mechanical and thermal properties. Consequently, a substantial body of literature, encompassing both theoretical and experimental studies, has been dedicated to fracture mechanics, thermal stress distributions, and the various processing methods of these materials.

Several studies [3-7]have addressed the vibration characteristics of spherical structures by examining the influence of mechanical boundary conditions, geometric parameters, including thickness and polar angles, material properties, the material length-scale parameter, temperature gradients, and specific heat capacity at constant volume on their natural frequencies. Mohamed Sekkal et al[8] examined Free vibration, Buckling and Bending investigation of bidirectional FG curved sandwich beams. Bharti et al.[9]introduced an advanced higher-order shear and normal deformation theory to analyse bending and free vibrations in functionally graded material sandwich shells. Dorduncu, Chung et al [10, 11] investigated the bending analysis of functionally graded (FG) plates using a refined zigzag theory. Abdelaziz Timesli , Foroutan et Dai [12, 13], provided a comprehensive analysis model for the buckling behavior of porous FGM cylindrical shells embedded within an elastic foundation. Nguyen et al [14] developed a simple and refined first-order shear deformation theory (FSDT) for the analysis of free vibration, static behavior, and bending of advanced composite plates, highlighting that this theory can also be extended to other structural configurations such as beams and shells made of advanced composite materials

the magneto-electro vibration analysis of a moderately thick double-curved sandwich panel with porous core and graphene platelets reinforced composite (GPLRC) based on the nonlocal strain gradient theory (NSGT) is investigated by Mohammad Ali Mohammadimehr et al [15]. Mota et al[16] examined the effect of porosity on the static response of functionally graded (FG) plates using first-order shear deformation theory (FSDT) combined with the finite element method. In a related study, Zhao et al [17]investigated the free vibration behavior of porous FG plates by employing FSDT in conjunction with the Rayleigh–Ritz method.. Rachid et al[18]and Hongyan et al. [19]investigated the free vibration behavior of thin doubly curved FGM sandwich shells based on a new shear deformation theory incorporating stretching effects. Stability Analysis of Imperfect Functionally Graded Sandwich Plates with Ceramic middle layer and Varied Boundary Edges using Efficient Kinematic model were studied by Tamrabet Abdelkader et al [20]. Duong et al [21]presented an iso-geometric approach for the free vibration analysis of bi-directional functionally graded porous doubly curved shallow microshells with variable length-scale parameters. Rachid Slimani et al[22]utilized a A novel quasi-3D refined high-order shear theory (HSDT) to examine the static bending analysis of porous functionally graded Plates.

Despite the significant advances reported in the literature, research on the static behavior of doubly curved functionally graded material (FGM) sandwich shells based on novel higher-order shear deformation theories remains relatively scarce. In particular, the effects of geometric parameters, curvature and thickness ratios, sandwich configurations, and through-thickness material gradation on the bending response have not yet been fully explored. Therefore, further investigations based on accurate, robust, and computationally efficient theoretical models are still required to provide a comprehensive understanding of the static behavior of these advanced shell structures. As a result, the overarching objective of this study is to provide a novel theory of higher-order shear deformation applicable to the static evaluation of FGM sandwich cylindrical shells. The proposed model accurately considers transverse shear deformation and meets the boundary criteria for zero transverse shear stress without shear correction components. For simply supported shells, analytical solutions are determined using Navier's method, and is obtained from the governing equation from the notion of virtual work. The numerical results are displayed to investigate the influence of the material distribution, geometry parameters, and sandwich configurations on the static response of the considered structures.

2. Material Properties of FGM Plates with different porosity distributions

Assume that the bi-curved shell of the FGM sandwich shown in Figure 1 with subscripts c and m is made of ceramic and metal, respectively. The x-axis principal radius of curvature of the shell is R1, whereas the y-axis principal radius of curvature is R2. where a, b, and h are the curve length and shell thickness, respectively. An arbitrary point on the shell along the x-, y-, and z-axes is represented by u, v, and w, respectively.

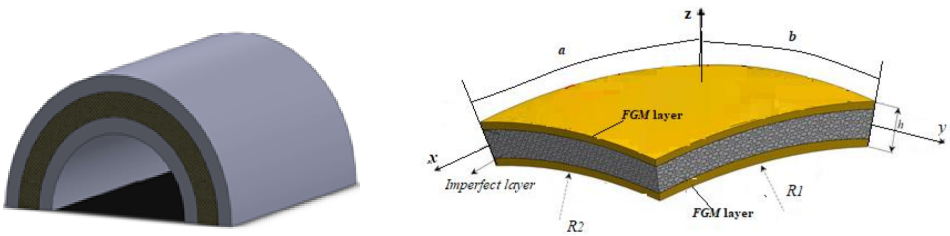

Fig 1: Geometry and coordinate systems of (a) porous FGM sandwich cylindrical shell - (b) functionally graded sandwich doubly-curved shell.

Table.1 displays the geometric creative specs for several shell types.

Table 1. The geometry creative specs for each type of shell (R = Curvature radius)

	Shell type	R_1	R_2
1	Cylindrical	R	∞
2	Spherical	R	R
3	Hyperbolic	R	$-R$

The material properties for each layer (n), such as the modulus of elasticity, Poisson's ratio (ν), and coefficient of thermal expansion (α), are assumed to be graded through thickness according to the power-law model of gradation [23].

$$P^{(n)}(z) = P_m + (P_c - P_m)V^{(n)} \tag{1}$$

As a function of the volume fraction $V(n)$, where $n = 1, 2,$ and 3, we obtain the following equation: $P(n)$ is the effective material property of the FGM of layer n, Pm is the property of the upper face of layer 1, and Pc is the property of the lower face of layer 3.

For a sandwich doubly-curved shell with FG face sheets, the volume fraction function $V(z)$ is displayed below[24]

$$\begin{aligned}
&V^{(1)}(z) = \left(\frac{z-h_0}{h_1-h_0}\right)^k && h_0 \le z \le h_1 \\
&V^{(2)}(z) = 1 && h_1 \le z \le h_2 \\
&V^{(3)}(z) = \left(\frac{z-h_3}{h_2-h_3}\right)^k && h_2 \le z \le h_3
\end{aligned} \tag{2}$$

The material variation profile through the functionally graded sandwich doubly-curved shell is indicated by the volume fraction index (k), which is ($0 \le k \le \infty$). In this study, we consider three characteristic porosity profiles for the core of functionally graded sandwich cylindrical shells, presented in Figure 2. The variables ρ(z) and E(z) represent the mass density and the elastic modulus of these structures, respectively, and are expressed as follows[25-28] :

Type 1 (P1): Uniform porosity distribution type

Type 2 (P2): Non-Uniform Porosity distribution type (Stiffer Surfaces)

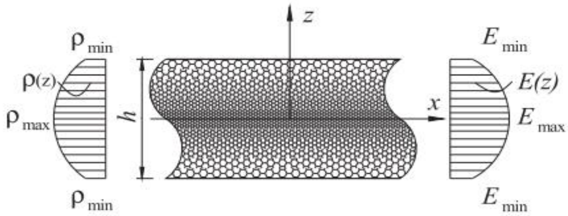

Type 3 (P3): Non-Uniform Porosity distribution type (Softer Surfaces)

Fig 2: Three typical porosity distribution profiles for functionally graded sandwich cylindrical shells

Type 1 (P1): Uniform porosity distribution type

$$E(z)=E_{\max}\left(\frac{2}{\pi}\sqrt{1-\zeta}-\frac{2}{\pi}+1\right)^{2}$$
$$\rho(z)=\rho_{\max}\left(\frac{2}{\pi}\sqrt{1-\zeta}-\frac{2}{\pi}+1\right) \tag{2a}$$

Type 2 (P2): Non-Uniform Porosity distribution type (Stiffer Surfaces)

$$E(z)=E_{\max}\left(1-\zeta\cos(\frac{\pi z}{h})\right)$$
$$\rho(z)=\rho_{\max}\left(1-\zeta_{m}\cos(\frac{\pi z}{h})\right) \tag{2b}$$

Type 3 (P3): Non-Uniform Porosity distribution type (Softer Surfaces)

$$E(z)=E_{\max}\left(1-\zeta\cos\left(\left|\frac{\pi z}{h}\right|-\frac{\pi}{2}\right)\right)$$
$$\rho(z)=\rho_{\max}\left(1-\zeta_{m}\cos\left(\left|\frac{\pi z}{h}\right|-\frac{\pi}{2}\right)\right) \tag{2c}$$

where ρ_{max} and E_{max} are the maximum values of mass density and Young's modulus, respectively; ζ and $\zeta_m=1-\sqrt{1-\zeta}$ are the porosity parameters and mass density, respectively.

3. Governing equations

With the use of higher-order l shell deformation theory, we can find the displacement field at any point z from the center surface. This is how the displacement field is described:

$$u(x,y,z)=(1+\frac{z}{R_x})u_0(x,y)-z\frac{\partial w_0}{\partial x}+K_1Af(z)\frac{\partial\theta}{\partial x}$$
$$v(x,y,z)=(1+\frac{z}{R_y})v_0(x,y)-z\frac{\partial w_0}{\partial y}+K_2Bf(z)\frac{\partial\theta}{\partial y} \tag{3}$$
$$w(x,y,z)=w_0(x,y,t)$$

$u0$, $v0$ and $w0$ are the mid-plane displacements, the coefficients K1 and K2 depend on the geometry.

With $$k_1 = \lambda^2, \quad k_2 = \mu^2, \quad A = -\frac{1}{\lambda^2}, \quad B = -\frac{1}{\mu^2} \tag{4a}$$

Where $$\lambda = \frac{m\pi}{a}, \; \mu = \frac{n\pi}{b} \tag{4b}$$

introduced. The specific form of the shape function *f(z)* is given by M. Chitour et al [29]

$$f(z) = \frac{3}{25}\pi z(\pi - \sqrt[3]{0.135}\cosh(\frac{\pi z}{h})) \tag{5}$$

The Using the theory of elasticity, the strain expressions obtained from the displacement field, as given in equations (3), can be written as follows:

$$\begin{aligned}
\varepsilon_{xx} &= \varepsilon_{xx}^0 + zk_x^1 + f(z)k_x^2, \\
\varepsilon_{yy} &= \varepsilon_{yy}^0 + zk_y^1 + f(z)k_y^2, \\
\gamma_{xy} &= \gamma_{xy}^0 + zk_{xy}^1 + f(z)k_{xy}^2, \\
\gamma_{yz} &= \frac{\partial f(z)}{\partial z}\gamma_{yz}^0, \\
\gamma_{xz} &= \frac{\partial f(z)}{\partial z}\gamma_{xz}^0,
\end{aligned} \tag{6}$$

Where

$$\begin{Bmatrix} \varepsilon_x^0 \\ \varepsilon_y^0 \\ \gamma_{xy}^0 \end{Bmatrix} = \begin{Bmatrix} \dfrac{\partial u_0}{\partial x} + \dfrac{w_0}{R_1} \\ \dfrac{\partial v_0}{\partial y} + \dfrac{w_0}{R_2} \\ \partial u_0 / \partial y + \partial v_0 / \partial x \end{Bmatrix}, \quad \begin{Bmatrix} k_x^1 \\ k_y^1 \\ k_{xy}^1 \end{Bmatrix} = \begin{Bmatrix} -\partial^2 w_0 / \partial x^2 \\ -\partial^2 w_0 / \partial y^2 \\ -2\partial^2 w_0 / \partial x \partial y \end{Bmatrix},$$

$$\begin{Bmatrix} k_x^2 \\ k_y^2 \\ k_{xy}^2 \end{Bmatrix} = \begin{Bmatrix} K_1 A \dfrac{\partial^2 \theta}{\partial x^2} \\ K_2 B \dfrac{\partial^2 \theta}{\partial y^2} \\ (k_1 A + k_2 B)\dfrac{\partial^2 \theta}{\partial x \partial y} \end{Bmatrix}, \begin{Bmatrix} \gamma_{xz}^0 \\ \gamma_{yz}^0 \end{Bmatrix} = \begin{Bmatrix} K_1 A \dfrac{\partial \theta}{\partial x} \\ K_2 B \dfrac{\partial \theta}{\partial y} \end{Bmatrix}, \tag{7}$$

And $$g(z) = \frac{df(z)}{dz}$$

The stress-strain relationships which take into account transverse shear and normal strains can be expressed as:

$$\begin{Bmatrix} \sigma_{xx} \\ \sigma_{yy} \\ \sigma_{yz} \\ \sigma_{xz} \\ \sigma_{xy} \end{Bmatrix}^{(n)} = \begin{bmatrix} Q_{11} & Q_{12} & 0 & 0 & 0 \\ Q_{12} & Q_{22} & 0 & 0 & 0 \\ 0 & 0 & Q_{44} & 0 & 0 \\ 0 & 0 & 0 & Q_{55} & 0 \\ 0 & 0 & 0 & 0 & Q_{66} \end{bmatrix}^{(n)} \begin{Bmatrix} \varepsilon_{xx} \\ \varepsilon_{yy} \\ \gamma_{yz} \\ \gamma_{xz} \\ \gamma_{xy} \end{Bmatrix} \tag{8}$$

The stiffness coefficients *(Qij)* are expressed as follows[30]

$$\begin{gathered} Q_{11}^{(n)} = Q_{22}^{(n)} = \frac{E^{(n)}(z)}{1-(\nu^{(n)})^2}, \\ Q_{12}^{(n)} = \nu^{(n)} Q_{11}^{(n)}, \\ Q_{44}^{(n)} = Q_{55}^{(n)} = Q_{66}^{(n)} = \frac{E^{(n)}(z)}{2(1+\nu^{(n)})} \end{gathered} \tag{9}$$

4. Equilibrium equations

Taking into account the static representation of the virtual work concept, we can derive the following expressions:

$$0 = \int_{-h/2}^{h/2} \left[\int_A \iint \sigma_{xx}\, \delta\varepsilon_{xx} + \sigma_{yy}\, \delta\varepsilon_{yy} + \tau_{xy}\, \delta\gamma_{xy} + \tau_{yz}\, \delta\gamma_{yz} + \tau_{xz}\, \delta\gamma_{xz} dA \right] dz - \int_A q\delta w\, dA \tag{10}$$

Replace the equations (6) and equations (8) into equations (12), and integrating through the thickness of the plate, equations (10) can be rewritten as:

$$0 = \int_A \begin{pmatrix} N_{xx}\delta\varepsilon_x^0 + N_{yy}\delta\varepsilon_y^0 + N_{xy}\delta\gamma_{xy}^0 + M_{xx}\delta k_x^1 + M_{yy}\delta k_y^1 + M_{xy}\delta k_x^1 \\ +P_{xx}\delta k_x^2 + P_{yy}\delta k_y^2 + P_{xy}\delta k_{xy}^2 + Q_{yz}\gamma_{yz}^0 + Q_{yz}\gamma_{xz}^0 - q\delta w_0 \end{pmatrix} dA \tag{11}$$

the following integrations provide *Ni, Mi, Pi*, and *Qi* is the distributed transverse load:

$$\begin{gathered} \begin{bmatrix} N_x & N_y & N_{xy} \\ M_x & M_y & M_{xy} \\ P_x & P_y & P_{xy} \end{bmatrix} = \sum_{n=1}^{3} \int_{h_n}^{h_{n+1}} (\sigma_x, \sigma_y, \tau_{xy}) \begin{Bmatrix} 1 \\ z \\ f(z) \end{Bmatrix} dz, \\ (Q_{xz}, Q_{yz}) = \sum_{n=1}^{3} \int_{h_n}^{h_{n+1}} (\tau_{xz}, \tau_{yz}) \frac{\partial f(z)}{\partial z} dz \end{gathered} \tag{12}$$

After inputting the values of $\delta u0$, $\delta v0$, $\delta w0$, and $\delta\theta$ into equations (11) using partial integration, the following doubly-curved shell governing equations are derived:

$$
\begin{aligned}
&\delta u_0: && \frac{\partial N_{xx}}{\partial x}+\frac{\partial N_{xy}}{\partial y}=0 \\
&\delta v_0: && \frac{\partial N_{xy}}{\partial x}+\frac{\partial N_{yy}}{\partial y}=0 \\
&\delta w_0: && \frac{\partial^2 M_{xx}}{\partial x^2}+2\frac{\partial^2 M_{xy}}{\partial x\partial y}+\frac{\partial^2 M_{yy}}{\partial y^2}-\frac{N_{xx}}{R_1}-\frac{N_{yy}}{R_2}=0 \\
&\delta\theta: && -K_1A\frac{\partial^2 P_{xx}}{\partial x^2}-K_2B\frac{\partial^2 P_{yy}}{\partial y^2}-(K_1A+K_2B)\frac{\partial^2 P_{xy}}{\partial x\partial y}+K_1A\frac{\partial Q_{xz}}{\partial x\partial z}+K_2B\frac{\partial Q_{yz}}{\partial y\partial z}=0
\end{aligned}
\tag{13}
$$

By By substituting equations (6) and equations (8) into equations (12), the stress resultants can be expressed in matrix form as follows

$$
\begin{Bmatrix} N_{xx} \\ N_{yy} \\ N_{xy} \\ M_{xx} \\ M_{yy} \\ M_{xy} \\ P_{xx} \\ P_{yy} \\ P_{xy} \end{Bmatrix}
=
\begin{bmatrix}
A_{11} & A_{12} & 0 & B_{11} & B_{12} & 0 & Cs_{11} & Cs_{12} & 0 \\
A_{12} & A_{22} & 0 & B_{12} & B_{22} & 0 & Cs_{12} & Cs_{22} & 0 \\
0 & 0 & A_{66} & 0 & 0 & B_{66} & 0 & 0 & Cs_{66} \\
B_{11} & B_{12} & 0 & D_{11} & D_{12} & 0 & F_{11} & F_{12} & 0 \\
B_{12} & B_{22} & 0 & D_{12} & D_{22} & 0 & F_{12} & F_{22} & 0 \\
0 & 0 & B_{66} & 0 & 0 & D_{66} & 0 & 0 & F_{66} \\
Cs_{11} & Cs_{12} & 0 & F_{11} & F_{12} & 0 & H_{11} & H_{12} & 0 \\
Cs_{12} & Cs_{22} & 0 & F_{12} & F_{22} & 0 & H_{12} & H_{22} & 0 \\
0 & 0 & Cs_{66} & 0 & 0 & F_{66} & 0 & 0 & H_{66}
\end{bmatrix}
\begin{Bmatrix} \varepsilon_{xx}^0 \\ \varepsilon_{xx}^0 \\ \gamma_{xy}^0 \\ \varepsilon_x^1 \\ \varepsilon_y^1 \\ \varepsilon_{xy}^1 \\ \varepsilon_x^2 \\ \varepsilon_y^2 \\ k_{xy}^2 \end{Bmatrix}
\tag{14}
$$

$$
\begin{Bmatrix} Q_{yz} \\ Q_{yz} \end{Bmatrix}
=
\begin{bmatrix} A_{44} & 0 \\ 0 & A_{55} \end{bmatrix}
\begin{Bmatrix} \gamma_{yz}^0 \\ \gamma_{xz}^0 \end{Bmatrix}
\tag{15}
$$

substituting Given that equations (7), equations (12), equations (14), and equations (15) are substituted into equations (13), the equations that regulate equilibrium are expressed as follows:

$$
\begin{aligned}
\delta u_0: {} & A_{11}\frac{\partial^2 u_0}{\partial x^2}+A_{66}\frac{\partial^2 u_0}{\partial y^2}+(A_{12}+A_{66})\frac{\partial^2 v_0}{\partial x\partial y}-B_{11}\frac{\partial^3 w_0}{\partial x^3}-(B_{12}+2B_{66})\frac{\partial^3 w_0}{\partial x\partial y^2}+Cs_{11}K_1A\frac{\partial^3\theta}{\partial x^3} \\
& +(Cs_{12}K_2B+Cs_{66}(K_1A+K_2B))\frac{\partial^3\theta}{\partial x\partial y^2}+\frac{\partial w_0}{\partial x}\left(\frac{A_{11}}{R_1}+\frac{A_{12}}{R_2}\right)=0
\end{aligned}
\tag{16a}
$$

$$
\begin{aligned}
\delta v_0: {} & (A_{12}+A_{66})\frac{\partial^2 u_0}{\partial x\partial y}+A_{22}\frac{\partial^2 v_0}{\partial y^2}+A_{66}\frac{\partial^2 v_0}{\partial x^2}-B_{22}\frac{\partial^3 w_0}{\partial y^3}-(B_{12}+2B_{66})\frac{\partial^3 w_0}{\partial x^2\partial y}+Cs_{22}K_2B\frac{\partial^3\theta}{\partial y^3} \\
& +(Cs_{12}K_1A+Cs_{66}(K_1A+K_2B))\frac{\partial^3\theta}{\partial x^2\partial y}+\frac{\partial w_0}{\partial x}\left(\frac{A_{12}}{R_1}+\frac{A_{22}}{R_2}\right)=0
\end{aligned}
\tag{16b}
$$

$$
\begin{aligned}
\delta w_0: \quad & B_{11}\frac{\partial^3 u_0}{\partial x^3}+(B_{12}+2B_{66})\frac{\partial^3 u_0}{\partial x\partial y^2}-\frac{\partial u_0}{\partial x}\left(\frac{A_{11}}{R_1}+\frac{A_{12}}{R_2}\right)+B_{22}\frac{\partial^3 v_0}{\partial y^3}+(B_{12}+2B_{66})\frac{\partial^3 v_0}{\partial x^2\partial y}\\
&-\frac{\partial v_0}{\partial x}\left(\frac{A_{12}}{R_1}+\frac{A_{22}}{R_2}\right)-D_{11}\frac{\partial^4 w_0}{\partial x^4}-D_{22}\frac{\partial^4 w_0}{\partial y^4}-(B_{12}+2B_{66})\frac{\partial^4 w_0}{\partial x^2\partial y^2}+2\left(\frac{A_{11}}{R_1}+\frac{A_{12}}{R_2}\right)\frac{\partial^2 w_0}{\partial x^2}\\
&+2\left(\frac{A_{12}}{R_1}+\frac{A_{22}}{R_2}\right)\frac{\partial^2 w_0}{\partial y^2}-2\left(\frac{A_{11}}{R_1^2}+\frac{A_{22}}{R_2^2}+2\frac{A_{12}}{R_1R_2}\right)w_0+F_{11}K_1A\frac{\partial^4\theta}{\partial x^4}+F_{22}K_2B\frac{\partial^4\theta}{\partial y^4}\\
&+(F_{12}+2F_{66})(K_1A+K_2B)\frac{\partial^4\theta}{\partial x^2\partial y^2}-\left(\frac{Cs_{11}}{R_1}+\frac{Cs_{12}}{R_2}\right)K_1A\frac{\partial^2\theta}{\partial x^2}-\left(\frac{Cs_{12}}{R_1}+\frac{Cs_{22}}{R_2}\right)K_2B\frac{\partial^2\theta}{\partial y^2}=0
\end{aligned}
\tag{16c}
$$

$$
\begin{aligned}
\delta\theta: \quad & -Cs_{11}K_1A\frac{\partial^3 u_0}{\partial x^3}-(Cs_{12}K_2B+Cs_{66}(K_1A+K_2B))\frac{\partial^3 u_0}{\partial x\partial y^2}-(Cs_{12}K_1A+Cs_{66}(K_1A+K_2B))\frac{\partial^3 v_0}{\partial x^2\partial y}\\
&-Cs_{22}K_2B\frac{\partial^3 v_0}{\partial x^3}+F_{11}K_1A\frac{\partial^4 w_0}{\partial x^4}+F_{22}K_2B\frac{\partial^4 w_0}{\partial y^4}+(K_1A+K_2B)(F_{12}+2F_{66})\frac{\partial^4 w_0}{\partial x^2\partial y^2}\\
&+\left(\frac{Cs_{11}}{R_1}+\frac{Cs_{12}}{R_2}\right)K_1A\frac{\partial^2 w_0}{\partial x^2}+\left(\frac{Cs_{12}}{R_1}+\frac{Cs_{22}}{R_2}\right)K_2B\frac{\partial^2 w_0}{\partial y^2}-H_{11}(K_1A)^2\frac{\partial^4\theta}{\partial x^4}H_{22}(K_2B)^2\frac{\partial^4\theta}{\partial y^4}\\
&-(2H_{12}K_1AK_2B+H_{66}(K_1A+K_2B)^2)\frac{\partial^4\theta}{\partial x^2\partial x^2}+A_{44}(K_1A)^2\frac{\partial^2\theta}{\partial x^2}+A_{55}(K_2B)^2\frac{\partial^2\theta}{\partial y^2}=0
\end{aligned}
\tag{16d}
$$

5. Solution approach for simply supported FG sandwich doubly-curved shell

Among the analytical methods reported in the literature, Navier's method represents one of the most straightforward approaches for investigating the static response of simply supported shells. Using this technique, the displacement variables that satisfy the aforementioned boundary conditions can be expressed in the form of **Fourier series** as follows:

$$
\begin{Bmatrix} u_0 \\ v_0 \\ w_0 \\ \theta \end{Bmatrix}=\sum_{m=1}^{\infty}\sum_{n=1}^{\infty}\begin{Bmatrix} U\cos(\lambda x)\sin(\mu y) \\ V\sin(\lambda x)\cos(\mu y) \\ W\sin(\lambda x)\sin(\mu y) \\ X\sin(\lambda x)\sin(\mu y) \end{Bmatrix}
\tag{17}
$$

Where:

λ=mπ/a, μ=nπ/b; U, V, W et *X* are arbitrary parameters to be determined. The transverse distributed load *q(x,y)* is also expanded double Fourier series as;

$$
q(x,y)=\sum_{m=1}^{\infty}\sum_{n=1}^{\infty}q_0\sin(\lambda x)\sin(\mu y)
\tag{18}
$$

In Equations of equilibrium (13) we substitute the stress and moment resultants from equations (14,15) and (17) to yield closed-form solutions for FGM doubly-curved shell bending problems.

$$
[L]\{\Delta\}=\{P\}
\tag{19}
$$

$$[L]=\begin{bmatrix} L_{11} & L_{12} & L_{13} & L_{14} \\ L_{12} & L_{22} & L_{23} & L_{24} \\ L_{13} & L_{23} & L_{33} & L_{34} \\ L_{14} & L_{24} & L_{34} & L_{44} \end{bmatrix},\quad \{P\}=\begin{Bmatrix} 0 \\ 0 \\ q \\ 0 \end{Bmatrix},\ \{\Delta\}=\{U,V,W,X\}^T \tag{20}$$

With:

$$\begin{aligned}
S_{11} &= A_{11}\lambda^2 + A_{66}\mu^2 \\
S_{12} &= (A_{12}+A_{66})\lambda\mu \\
S_{13} &= -B_{11}\lambda^3 - (B_{12}+2B_{66})\lambda\mu^2 - (\frac{A_{11}}{R_1}+\frac{A_{12}}{R_2})\lambda \\
S_{14} &= Cs_{11}K_1A\lambda^3 + (Cs_{12}K_2B + Cs_{66}(K_1A+K_2B))\lambda\mu^2 \\
S_{22} &= A_{22}\mu^2 + A_{66}\lambda^3 \\
S_{23} &= -B_{22}\mu^3 - (B_{12}+2B_{66})\lambda^2\mu - (\frac{A_{12}}{R_1}+\frac{A_{22}}{R_2})\mu \\
S_{24} &= Cs_{22}K_2B\,\mu^3 + (Cs_{12}K_1A + Cs_{66}(K_1A+K_2B))\lambda^2\mu \\
S_{33} &= -D_{11}\lambda^4 - D_{22}\mu^4 - 2(D_{12}+2D_{66})\lambda^2\mu^2 + 2(\frac{B_{11}}{R_1}+\frac{B_{12}}{R_2})\lambda^2 + 2(\frac{B_{12}}{R_1}+\frac{B_{22}}{R_2})\mu^2 \\
&\quad + (\frac{A_{11}}{R_1^{\,2}}+\frac{A_{22}}{R_2^{\,2}}+2\frac{A_{12}}{R_1^{\,2}R_2^{\,2}}) \\
S_{34} &= F_{11}K_1A\lambda^4 + F_{22}K_2B\mu^4 + (F_{12}+2F_{66})(K_1A+K_2B))\lambda^2\mu^2 + (\frac{Cs_{11}}{R_1}+\frac{Cs_{12}}{R_2})\lambda^2K_1A \\
&\quad + (\frac{Cs_{12}}{R_1}+\frac{Cs_{22}}{R_2})\mu^2K_2B \\
S_{44} &= -(2H_{12}K_1AK_2B + H_{66}(K_1A+K_2B)^2
\end{aligned} \tag{21}$$

6. Convergence and validation study

The bending analysis of a simple supported FGM doubly curved shell is presented as follows. Sinusoidal and uniform loads are analysed, and many numerical examples are provided and discussed to verify the accuracy of the shear deformation theory used to analyse the static bending of the FGM sandwich doubly curved shell. This study examined an alumina-composite FGM sandwich with a doubly curved shell. (*Al2O3*) as the ceramic phase and aluminum (Al) as the metal phase. Values of parameters for these materials are presented in Table.1[31-33]

Table 2. The properties of the materials used for FGM sandwich doubly-curved shell

Materials	Mechanical proprieties		
	E (GPa)	α *(K^{-1})*	υ
Al	*70*	*$23*10^{-6}$*	*0.3*
Al_2O_3	*380*	*$7*10^{-6}$*	*0.3*

To facilitate the analysis, all results are presented in a non-dimensional form, which allows easier comparison and improves their understanding. The following non-dimensional form is used to display the highest values of transverse displacements and stresses.

$$\bar{w}=\frac{100h^3E_0}{q_0a^4}w\left(\frac{a}{2},\frac{b}{2},0\right),\ \bar{\sigma}_x=\frac{h}{q_0a}\sigma_x\left(\frac{a}{2},\frac{b}{2},-\frac{h}{2}\right),$$
$$\bar{\tau}_{xz}=\frac{h}{q_0a}\tau_{xz}\left(0,\frac{b}{2},\frac{z}{h}\right),E_0=1 \tag{22}$$

This We compared our findings to those already published in the literature to ensure that our proposed formulation is correct. Consequently, merely supported FGM sandwich cylindrical shells have been considered. In this case, we consider $a = R$, $a/h = 10$, $R = R_1$; $R_2 = \infty$, $k=1,2$, $E_0 = 1$.

Under a sinusoidal transverse load, Table3-5 displays the primary findings for several FGM sandwich cylindrical shells with respect to transverse displacements and stresses. The tables indicate that our suggested formulation yields results that closely match those predicted by Shinde and Sayyad. and Atteshamuddin S. Sayyad [34, 35], respectively. The results in Table 3-5 show how the non-dimensional transverse displacements and stresses change for SS FGM sandwich shells with different power-law indices k and layer schemes. Additionally, an increase in the power law index is associated with a increase in the transverse displacements and stresses

Table 3 Comparison of non-dimensional transverse displacements of FGM sandwich cylindrical shells subjected to sinusoidal load comprised of FGM (R1 = R, R2 = ∞, R/a =1, a/h=10).

k	Theory	FGM Sandwich Schemes			
		1-0-1	2-1-2	1-1-1	1-2-1
1	PSDT[35]	0.9324	0.8221	0.7520	0.6680
	TSDT[35]	0.9323	0.8220	0.7520	0.6680
	HSDT[35]	0.9324	0.8221	0.7520	0.6679
	ESDT[35]	0.9322	0.8219	0.7519	0.6679
	Shinde and Sayyad[34]	0.8970	0.7907	0.7234	0.6430
	Present	**0.9335**	**0.8230**	**0.7529**	**0.6688**
2	PSDT[35]	1.2750	1.0553	0.9258	0.7797
	TSDT[35]	1.2747	1.0551	0.9257	0.7797
	HSDT[35]	1.2750	1.0553	0.9258	0.7797
	ESDT[35]	1.2745	1.0553	0.9257	0.7797
	Shinde and Sayyad[34]	1.2258	1.0135	0.8891	0.7493
	Present	**1.2761**	**1.0560**	**0.9265**	**0.7805**

Table 4. Comparison of non-dimensional normal stresses FGM sandwich cylindrical shells subjected to sinusoidal load comprised of FGM (*R1 = R, R2 = ∞, R/a =1, a/h=10*).

k	Theory	FGM Sandwich Schemes			
		1-0-1	2-1-2	1-1-1	1-2-1
1	PSDT[35]	0.6119	0.5395	0.4932	0.4372
	TSDT[35]	0.6121	0.5393	0.4934	0.4369
	HSDT[35]	0.6119	0.5395	0.4932	0.4372
	ESDT[35]	0.6124	0.5399	0.4935	0.4375
	Shinde and Sayyad[34]	0.6034	0.5319	0.4866	0.4322
	Present	0.6130	0.5406	0.4940	0.4380
2	PSDT[35]	0.8392	0.6952	0.6095	0.5121
	TSDT[35]	0.8395	0.6949	0.6097	0.5119
	HSDT[35]	0.8391	0.6952	0.6095	0.5121
	ESDT[35]	0.8397	0.6961	0.6099	0.5125
	Shinde and Sayyad[34]	0.8245	0.6813	0.5975	0.5036
	Present	0.8408	0.6966	0.6107	0.5131

able 5. Comparison of non-dimensional transverse shear stress of FGM sandwich cylindrical shells subjected to sinusoidal load comprised of FGM *(R1 = R, R2 = ∞, R/a =1, a/h=10).*

k	Theory	FGM Sandwich Schemes			
		1-0-1	2-1-2	1-1-1	1-2-1
1	PSDT[35]	0.1590	0.1399	0.1333	0.1301
	TSDT[35]	0.1622	0.1429	0.1366	0.1339
	HSDT[35]	0.1590	0.1396	0.1330	0.1297
	ESDT[35]	0.1654	0.1460	0.1399	0.1378
	Shinde and Sayyad[34]	0.1386	0.1250	0.1242	0.1284
	Present	0.1654	0.1452	0.1383	0.1351
2	PSDT[35]	0.1831	0.1429	0.1313	0.1265
	TSDT[35]	0.1854	0.1451	0.1314	0.1299
	HSDT[35]	0.1831	0.1427	0.1311	0.1262
	ESDT[35]	0.1877	0.1429	0.1366	0.1334
	Shinde and Sayyad[34]	0.1427	0.1198	0.1154	0.1231
	Present	0.1902	0.1477	0.1353	0.1302

Table.6. Comparison of Dimensionless transverse displacements of FGM (Al/ZrO2) cylindrical shells under uniform load

Type of shell	Theory	Model	Power-law index k					
			$k = 0$	$k = 0.2$	$k = 0.5$	$k = 1$	$k = 2$	$k = 5$
CY shells (Rx/a = 1, Ry/b = ∞)	S. Benounas[36]	SQ8-IFSDT	0.0427	0.0481	0.0543	0.0608	0.0667	0.0726
	Zhao et al[37]	FSDT	0.0427	0.0481	0.0543	0.0608	0.0667	0.0725
	Viola et al[38]	UTSDT	0.0429	0.0483	0.0546	0.0611	0.0670	0.0728
	Rachid et al[18]	HSDT	0.0439	0.0495	0.0559	0.0626	0.0687	0.0746
	Amina A B et al[39]	HSDT	0.0441	0.0497	0.0561	0.0628	0.0689	0.0749
	Present	**HSDT**	**0.0429**	**0.0479**	**0.0537**	**0.0602**	**0.0673**	**0.0749**

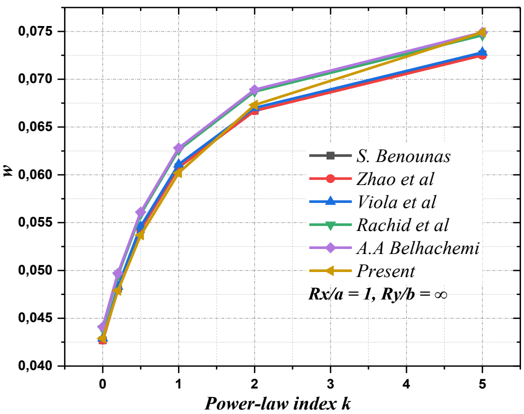

Fig. 3. Comparison of non-dimensional deflection along the Power-law index k of simply supported FGM sandwich cylindrical shells *(a=b=10h, R1=a, R2= ∞)*

Table 6 and Fig. 3 present a comparative study of the dimensionless transverse displacements of functionally graded material FGM cylindrical (*CY*) shells subjected to a uniformly distributed load. These structures are composed of a mixture of Aluminium (*Al*) and Zirconium Dioxide (*ZrO_2*). The results presented in the table and figure successfully validate the accuracy of the proposed Higher-Order Shear Deformation Theory (*HSDT*) formulation. They demonstrate that the present model accurately captures the complex mechanical behavior of FGM cylindrical shells and confirm the significant influence of material gradation, governed by the power-law index *k*, on the structural stiffness.

Table.7. Comparison of non-dimensional deflection and stress of simply supported *Al/Al2O3* cylindrical shells under sinusoidally distributed load *a=b=10h*

Mode	R_1/a	k	Method	*w* (0)	σ_x (1/2)	σ_{xz} (0)
Cylindrical R2 = ∞	**2**	**Ceramic**	Amina A B et al[39]	0.2602	1.9632	0.2530
			Present	0.2513	1.6817	0.2175
		1	Amina A B et al[39]	0.5076	3.1038	0.2614
			Present	0.4856	3.2778	0.2116
		5	Amina A B et al[39]	0.8127	4.4997	0.2073
			Present	0.7790	4.8262	0.1862
		Metal	Amina A B et al[39]	1.4126	1.9632	0.2530
			Present	1.3639	1.6827	0.2175
	5	**Ceramic**	Amina A B et al[39]	0.2895	2.0573	0.2463
			Present	0.2894	1.9372	0.2505
		1	Amina A B et al[39]	0.5754	3.2359	0.2481
			Present	0.5723	3.8608	0.2493
		5	Amina A B et al[39]	0.8965	4.5184	0.2004
			Present	0.8964	4.7991	0.2142
		Metal	Amina A B et al[39]	1.5719	2.0573	0.2463
			Present	1.5711	1.9472	0.2505

Table.8. Comparison of non-dimensional deflection and stress of simply supported *Al/Al2O3* Spherical shells under sinusoidally distributed load *a=b=10h*

Mode	R_1/a	k	Method	w (0)	σ_x (1/2)	σ_{xz} (0)
Spherical $R_2 = R_1$	2	Ceramic	Amina A B et al[39]	0.1765	1.5371	0.1866
			Present	0.1708	1.6825	0.1579
		1	Amina A B et al[39]	0.3291	2.3924	0.1930
			Present	0.3156	2.1293	0.1674
		5	Amina A B et al[39]	0.5556	3.7187	0.1575
			Present	0.5309	3.4929	0.1269
		Metal	Amina A B et al[39]	0.9585	1.5371	0.1866
			Present	0.9372	1.6825	0.1579
	5	Ceramic	Amina A B et al[39]	0.2671	2.0250	0.2308
			Present	0.2663	1.8825	0.2305
		1	Amina A B et al[39]	0.5254	3.2028	0.2352
			Present	0.5195	3.4046	0.2263
		5	Amina A B et al[39]	0.8320	4.5865	0.1917
			Present	0.8254	4.8312	0.1972
		Metal	Amina A B et al[39]	1.4502	2.0250	0.2308
			Present	1.4466	1.8825	0.2305

Table.9. Comparison of non-dimensional deflection and stress of simply supported *Al/Al2O3* Elliptical shells under sinusoidally distributed load *a=b=10h*

Mode	R_1/a	k	Method	w (0)	σ_x (1/2)	σ_{xz} (0)
Elliptical $R_2 = 2R_1$	2	Ceramic	Amina A B et al[39]	0.2158	1.7586	0.2112
			Present	0.2100	1.4657	0.1818
		1	Amina A B et al[39]	0.4120	2.7638	0.2180
			Present	0.3967	2.6765	0.1728
		5	Amina A B et al[39]	0.6780	4.1556	0.1772
			Present	0.6521	4.2903	0.1558
		Metal	Amina A B et al[39]	1.1718	1.7586	0.2112
			Present	1.1409	1.4657	0.1818
	5	Ceramic	Amina A B et al[39]	0.2794	2.0523	0.2379
			Present	0.2793	1.9695	0.2418
		1	Amina A B et al[39]	0.5529	3.2413	0.2411
			Present	0.5491	3.7041	0.2391
		5	Amina A B et al[39]	0.8677	4.5800	0.1958
			Present	0.8653	5.0948	0.2068
		Metal	Amina A B et al[39]	1.5165	2.0523	0.2379
			Present	1.5167	1.9695	0.2418

Tables 7, 8, and 9 demonstrate the significant impact of shell geometry, curvature radius ratio R_1/a, and volume fraction index k on the static response of FGM Al/Al_2O_3 shells. Increasing the metallic volume fraction k lowers the overall structural stiffness due to the inferior elastic modulus of aluminum relative to alumina, consequently amplifying the central transverse deflection w and internal stresses. Conversely, the double curvature inherent to the spherical shell $R_2=R_1$ yields a higher membrane stiffness compared to elliptical $R_2=2R_1$ and cylindrical $R_2=\infty$ geometries, which substantially mitigates central deformation. Ultimately, the excellent correlation between the present formulation and the reference data (Amina A. Belhachemi) confirms the reliability of the proposed numerical model for assessing the static behavior of such structures.

Table.10 non-dimensional transverse displacement (w) in FGM sandwich shells of double curvature under sinusoidal load *(a = b, a/h=10).*

Type of shell	*R1 /a*	*R2 /b*	Theory	FGM Sandwich Schemes							
				k = 1				k= 2			
				1–0–1	2–1–2	1–1–1	1–2–1	1–0–1	2–1–2	1–1–1	1–2–1
Spherical	1	1	PSDT[35]	0.3623	0.3188	0.2937	0.2655	0.4798	0.3910	0.3452	0.2978
			TSDT[35]	0.3623	0.3188	0.2937	0.2655	0.4797	0.3910	0.3452	0.2978
			HSDT[35]	0.3623	0.3188	0.2937	0.2655	0.4798	0.3910	0.3452	0.2978
			ESDT[35]	0.3623	0.3188	0.3188	0.2655	0.4797	0.3910	0.3910	0.2978
			Present	**0.3625**	**0.3190**	**0.2938**	**0.2657**	**0.4799**	**0.3911**	**0.3453**	**0.2979**
Hyperbolic	1	–1	PSDT[35]	1.9609	1.7349	1.5673	1.3498	2.8490	2.4333	2.1071	1.6924
			TSDT[35]	1.9604	1.7346	1.5671	1.3498	2.8479	2.4326	2.1067	1.6924
			HSDT[35]	1.9609	1.7350	1.5673	1.3498	2.8491	2.4334	2.1071	1.6923
			ESDT[35]	1.9597	1.7341	1.5669	1.3498	2.8465	2.4333	2.1063	1.6924
			Present	**1.9656**	**1.7390**	**1.5710**	**1.3530**	**2.8547**	**2.4374**	**2.1106**	**1.6956**

Elliptical	1	1.5	PSDT[35]	0.4825	0.4248	0.3907	0.3519	0.6432	0.5258	0.4637	0.3981
			TSDT[35]	0.4825	0.4248	0.3907	0.3519	0.6432	0.5258	0.4637	0.3981
			HSDT[35]	0.4825	0.4248	0.3907	0.3519	0.6432	0.5258	0.4637	0.3981
			ESDT[35]	0.4824	0.4247	0.3907	0.3519	0.6431	0.5258	0.4636	0.3981
			Present	**0.4828**	**0.4250**	**0.3910**	**0.3522**	**0.6435**	**0.5260**	**0.4638**	**0.3982**

Figure 4 presents the evolution of the dimensionless transverse displacement w as a function of the geometric span-to-thickness ratio (*a/h*) for simply supported functionally graded material (FGM) sandwich cylindrical shells subjected to a uniformly distributed load. The results are established for perfect and porous structures (Imperfect P1, P2, and P3), considering two core configurations (Type A: metallic core, Type B: ceramic core) as well as three laminations' schemes (2-1-2, 1-1-1, and 1-2-1). It is observed that the transverse displacement progressively decreases with the increase of the a/h ratio, reflecting the increase in overall stiffness associated with the reduction in the relative thickness of the structure. For all the studied configurations, the Type B shells exhibit systematically lower transverse displacements than the Type A shells, which highlights the beneficial effect of a ceramic core on the mechanical response. This behavior is directly linked to the high elastic modulus of the ceramic, which provides the structure with greater bending and membrane stiffness. On the other hand, the introduction of porosity leads to an increase in transverse displacement for all analyzed configurations. This trend is attributed to the decrease in effective elastic properties induced by the presence of pores, which reduces the overall stiffness of the structure and increases its deformability. Furthermore, this effect becomes more pronounced as the level of porosity increases, highlighting the significant influence of material imperfections on the static behavior of FGM sandwich cylindrical shells.

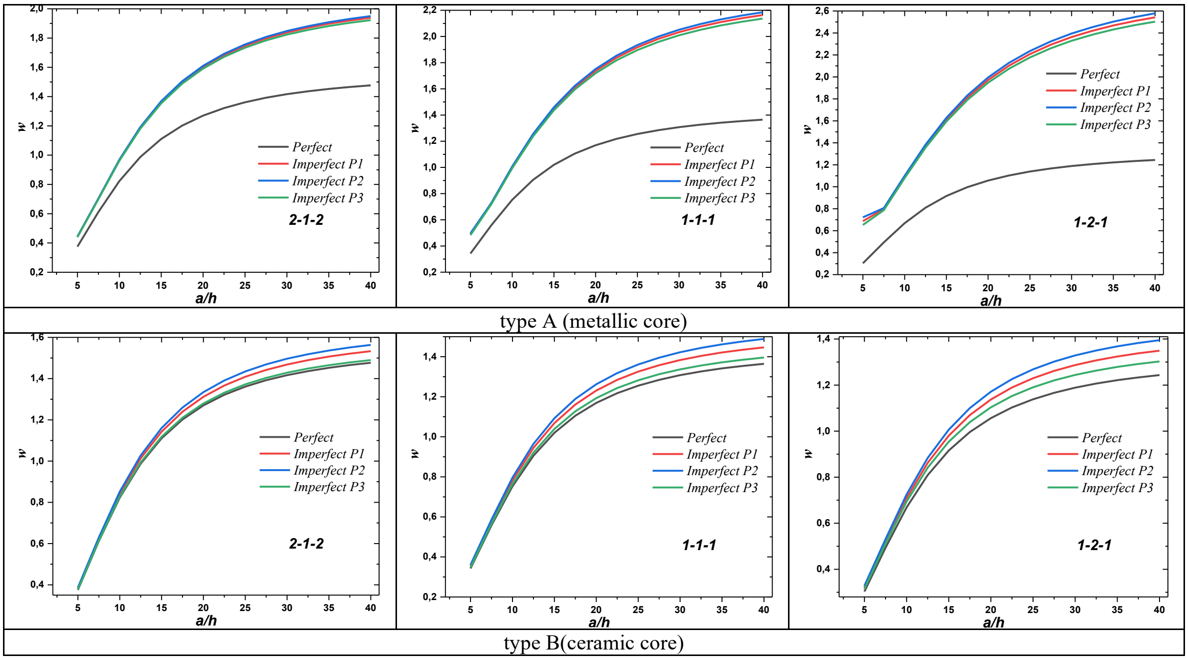

Fig.4: Variation of non-dimensional transverse displacement (w) along the span-to-thickness ratio a/h of simply supported perfect and porous sandwich cylindrical shells subjected to uniformly distributed load ***(k=1, a=b, R1=R, R=a, R2=*** ∞***,*** ζ ***=0.2)***

Figure 5 illustrates the evolution of the non-dimensional transverse displacement w of simply supported functionally graded material FGM sandwich cylindrical shells as a function of the porosity coefficient (ζ). The results are compared for different pore distributions (denoted as Imperfect P1, P2, and P3) and for two core configurations. It can be observed from these curves that the transverse displacement is highly dependent on the porosity coefficient and the layer arrangement configuration. Indeed, the introduction and increase of porosity enhance the structural flexibility, leading to a significant increase in the deflection. However, the adoption of a ceramic core (Type B) considerably reduces this deflection compared with a metallic core (Type A), due to its higher effective stiffness. Furthermore, the choice of the imperfection profile (P1, P2, P3) plays a critical role in controlling the overall elastic response of the FGM sandwich shell.

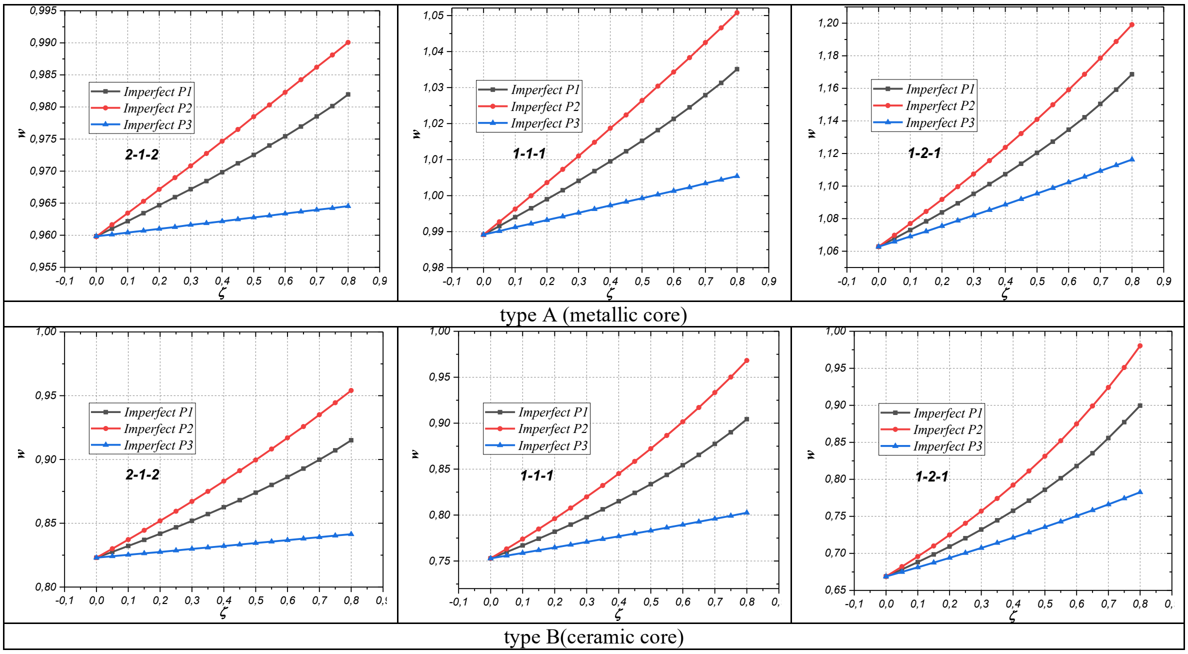

Fig 5 : Variation of non-dimensional transverse displacement (w) of simply supported FGM sandwich cylindrical shells *(a=b=10h, R1=a, R2= ∞)* with various porosity distribution types with respect to porosity coefficient

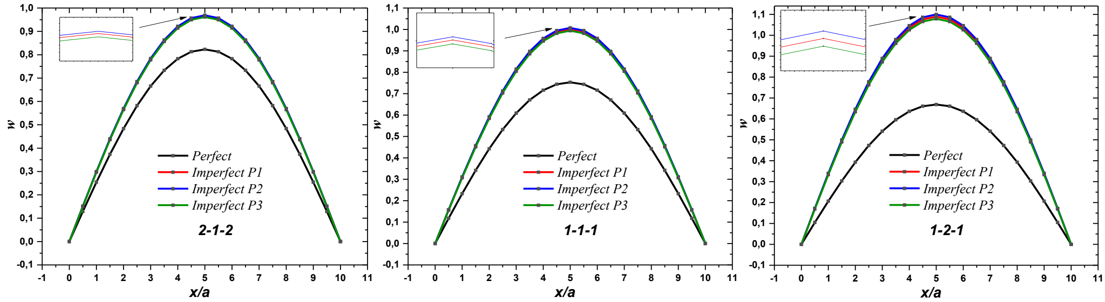

Fig 6 : Variation of non-dimensional transverse displacement (w) versus the length direction of simply supported perfect and FGM porous sandwich cylindrical shells subjected to uniformly distributed load *(k=1, a=b, R1=R, R=a, R2= ∞, ζ =0.2)*

Figure 6 show the influence of porosity imperfections on the overall stiffness of sandwich shells. The comparison between the "Perfect" and "Imperfect" profiles (P1, P2, and P3) clearly demonstrates the sensitivity of the structure to porosity defects. The presence of pores leads to a reduction in the overall stiffness, resulting in higher transverse displacements for the imperfect models compared with the perfect case.

The analysis of the results in Figure 7 highlights that the transverse displacement increases rapidly for low values of the geometric ratio R_1/a due to a loss of stiffness induced by the decrease in curvature, before stabilizing asymptotically as the structure degenerates to resemble a flat plate (for $R_1/a > 10$). Furthermore, the curves demonstrate a strict stiffness hierarchy depending on the layer configuration, with the (1-2-1) scheme minimizing displacement compared to the (1-1-1) and (2-1-2) arrangements. This behavior indicates that modifying the thickness of the ceramic layer improves the effective membrane stiffness of the sandwich shell. Finally, although the different porosity profiles (*P1, P2, P3*) cause slight variations in the maximum deflection amplitude, they do not affect the overall trends or the order of effectiveness of the thickness schemes, thus confirming that macro-geometry and structural arrangement largely predominate over the local distribution of microporosities.

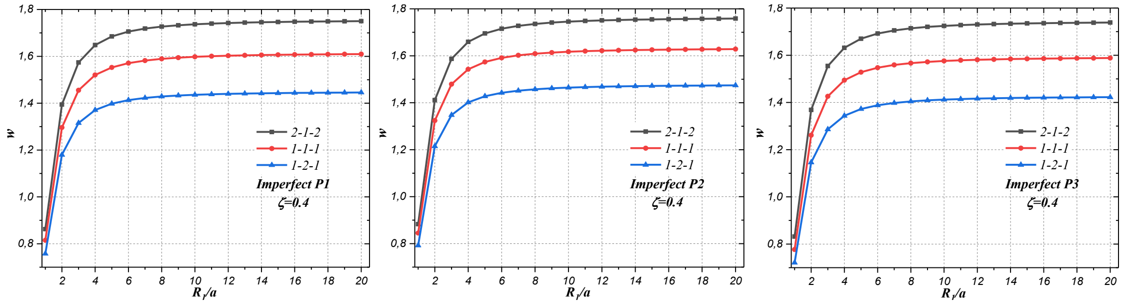

Fig 7: . Effect of the geometric ratio *R1/a* on the variation of the dimensionless transverse displacement (w) of simply supported FGM porous sandwich cylindrical shells subjected to uniformly distributed load *(k=1, a=b, R2= ∞, ζ =0.4).*

Figure 8 illustrates the distribution of the dimensionless transverse shear stress τ_{xz} through the thickness *z/h* for three-layer configurations (2-1-2, 1-1-1, and 1-2-1) and four porosity models (ζ = 0.4). For all cases considered, the shear stress rigorously vanishes at the outer surfaces, *z/h=0.5* (τ_{xz}= *0*), thereby confirming that the model satisfies the free-surface boundary conditions. Increasing the thickness of the porous core (from the 2-1-2 to the 1-2-1 configuration) broadens the parabolic profile and smooths the slope discontinuities at the layer interfaces. Finally, the introduction of porosity significantly modifies both the amplitude and distribution of τ_{xz} compared with the homogeneous/perfect case (perfect). The presence of voids reduces the local shear stiffness modulus. Depending on the type of pore distribution (Types 1, 2, and 3), these effects lead to noticeable variations in the transverse shear stress distribution.

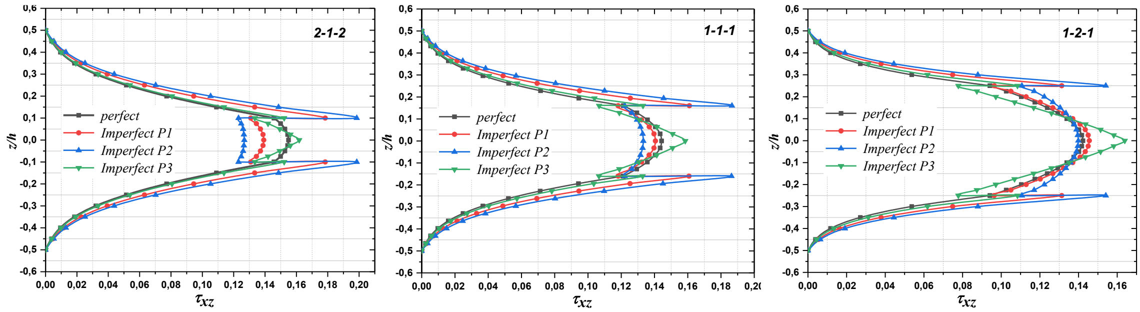

Fig 8: Through-the-thickness distribution of non-dimensional transverse shear stress for the FGM porous sandwich cylindrical shells subjected to uniformly distributed load (k=1, a=b, R2= ∞, ζ =0.4)

7. Conclusion

This study presented an analytical investigation of the static bending behavior of functionally graded material (FGM) sandwich cylindrical shells with porous cores based on a novel four-variable higher-order shear deformation theory (HSDT). The proposed formulation eliminates the need for a shear correction factor and employs the principle of virtual work in conjunction with Navier's method to derive the governing equilibrium equations for simply supported shells. The accuracy and reliability of the proposed model were verified through rigorous comparative and parametric analyses, showing very good agreement with available analytical results. The numerical findings demonstrate that the introduction of porosity reduces the overall structural stiffness, resulting in increased transverse displacements and enhanced structural deformability. Furthermore, sandwich configurations with a ceramic core exhibit greater bending resistance and lower transverse deflections than those with a metallic core, owing primarily to the higher elastic modulus of the ceramic material. Among the investigated layer arrangements, the 1-2-1 configuration provides the highest structural stiffness and minimizes the central transverse deflection. The results also confirm that both the porosity distribution and geometric parameters significantly affect the bending response and stress distribution of the shells. The through-thickness shear stress distributions further demonstrate that the proposed theory accurately satisfies the free-surface boundary conditions while effectively capturing the effects of porosity and layer configuration. Overall, the proposed refined two-dimensional theory provides an efficient and reliable framework for describing the complex interactions among material gradation, porosity imperfections, layer configuration, and internal stress fields. It can therefore serve as a useful analytical tool for the analysis, design, and optimization of advanced porous FGM sandwich shells for high-performance engineering applications.

References

[1] H.-T. Thai, S.-E. Kim, A review of theories for the modeling and analysis of functionally graded plates and shells, *Composite Structures,* Vol. 128, pp. 70-86, 2015.

[2] M. S. Ismail, J. Mahmud, O. Ifayefunmi, J. Purbolaksono, Buckling failures in curved shell structures: a comprehensive review of theory, design, and applications, *Journal of the Brazilian Society of Mechanical Sciences and Engineering,* Vol. 48, No. 2, pp. 83, 2026.

[3] M. Kholdi, G. Rahimi, A. Loghman, H. Ashrafi, M. Arefi, Analysis of thick-walled spherical shells subjected to various temperature gradients: thermo-elasto-plastic and residual stress studies, *International Journal of Applied Mechanics,* Vol. 13, No. 09, pp. 2150105, 2021.

[4] E. Sobhani, Vibrational characteristics of fastening of a spherical shell with a coupled conical-conical shells strengthened with nanocomposite sandwiches contained agglomerated CNT face layers and GNP core under spring boundary conditions, *Engineering Analysis with Boundary Elements,* Vol. 146, pp. 362-387, 2023.

[5] E. Sobhani, A. R. Masoodi, A. R. Ahmadi-Pari, Circumferential vibration analysis of nano-porous-sandwich assembled spherical-cylindrical-conical shells under elastic boundary conditions, *Engineering Structures,* Vol. 273, pp. 115094, 2022.

[6] S. Wang, S. Lin, A novelly universal theory: Toward accurately evaluating radial vibration characteristics for radially sandwiched spherical piezoelectric transducer, *Ultrasonics,* Vol. 111, pp. 106299, 2021.

[7] R. K. Yadav, S. S. Gupta, Inextensional vibrations of thin spherical shells using strain gradient elasticity theory, *Thin-Walled Structures,* Vol. 202, pp. 112061, 2024.

[8] M. Sekkal, W. Tebboune, O. Taleb, R. Bachir Bouiadjra, S. Benyoucef, A. Tounsi, Free vibration, Buckling and Bending investigation of bidirectional FG curved sandwich beams, *Journal of Computational Applied Mechanics,* Vol. 56, No. 3, pp. 641-662, 2025.

[9] B. M. Shinde, A. S. Sayyad, Static flexural analysis of imperfect FGM sandwich plates and shallow shells considering the effects of transverse normal strain, *Mechanics Based Design of Structures and Machines,* Vol. 54, No. 1, pp. 2602673, 2026.

[10] M. Dorduncu, Flexure analysis of functionally graded plates using {2, 2}-refined zigzag theory, *Journal of Aeronautics and Space Technologies,* Vol. 12, No. 1, pp. 19-30, 2019.

[11] C.-D. Chen, B.-F. Huang, A novel higher-order refined zigzag theory for static bending analysis in sandwich composite beam, *Applied Mathematical Modelling,* Vol. 119, pp. 586-604, 2023.

[12] A. Tımeslı, Analytical modeling of buckling behavior of porous FGM cylindrical shell embedded within an elastic foundation, *Gazi University Journal of Science,* Vol. 35, No. 1, pp. 148-165, 2022.

[13] K. Foroutan, L. Dai, Static and dynamic thermal post-buckling analysis of imperfect sigmoid FG cylindrical shells resting on a non-uniform elastic foundation, *European Journal of Mechanics-A/Solids,* Vol. 97, pp. 104770, 2023.

[14] H. N. Nguyen, T. T. Hong, P. V. Vinh, N. D. Quang, D. V. Thom, A refined simple first-order shear deformation theory for static bending and free vibration analysis of advanced composite plates, *Materials,* Vol. 12, No. 15, pp. 2385, 2019.

[15] M. A. Mohammadimehr, A. Loghman, S. Amir, M. Mohammadimehr, E. Arshid, Ö. Civalek, Magneto-electro vibration analysis of a moderately thick double-curved sandwich panel with porous core and GPLRC using FSDT, *Journal of Computational Applied Mechanics,* Vol. 56, No. 3, pp. 673-693, 2025.

[16] A. F. Mota, M. A. R. Loja, J. I. Barbosa, J. A. Rodrigues, Porous functionally graded plates: an assessment of the influence of shear correction factor on static behavior, *Mathematical and Computational Applications,* Vol. 25, No. 2, pp. 25, 2020.

[17] J. Zhao, Q. Wang, X. Deng, K. Choe, R. Zhong, C. Shuai, Free vibrations of functionally graded porous rectangular plate with uniform elastic boundary conditions, *Composites Part B: Engineering,* Vol. 168, pp. 106-120, 2019.

[18] A. Rachid, D. Ouinas, A. Lousdad, F. Z. Zaoui, B. Achour, H. Gasmi, T. A. Butt, A. Tounsi, Mechanical behavior and free vibration analysis of FG doubly curved shells on elastic foundation via a new modified

displacements field model of 2D and quasi-3D HSDTs, *Thin-Walled Structures,* Vol. 172, pp. 108783, 2022.

[19] H. Chen, A. Wang, Y. Hao, W. Zhang, Free vibration of FGM sandwich doubly-curved shallow shell based on a new shear deformation theory with stretching effects, *Composite Structures,* Vol. 179, pp. 50-60, 2017.

[20] A. Tamrabet, C. Mourad, N. Ali Alselami, A. Menasria, B. Mamen, A. Bouhadra, Efficient kinematic model for stability analysis of imperfect functionally graded sandwich plates with ceramic middle layer and varied boundary edges, *Journal of Computational Applied Mechanics,* Vol. 55, No. 2, pp. 184-200, 2024.

[21] K. D. Duong, D. N. Mai, P. V. Minh, T. V. Ke, An isogeometric approach to free vibration analysis of bi-directional functionally graded porous doubly-curved shallow microshells with variable length-scale parameters, *Frontiers of Structural and Civil Engineering,* Vol. 17, No. 12, pp. 1871-1894, 2023.

[22] R. Slimani, A. Menasria, M. Ali Rachedi, C. Mourad, S. Refrafi, A. A. Nimer, A. Bouhadra, B. Mamen, A novel quasi-3D refined HSDT for static bending analysis of porous functionally graded Plates, *Journal of Computational Applied Mechanics,* Vol. 55, No. 3, pp. 519-537, 2024.

[23] H. Benachi, A. Menasria, A. Bouhadra, S. Refrafi, M. Baazouzi, M. Chitour, N. Himeur, Instability Behavior of FG Nanoplates Resting on Nonlinear Kerr Foundations under Hygro-Thermo-Mechanical Load Using Nonlocal Elasticity Theory, *Mechanics of Solids,* Vol. 60, No. 8, pp. 7085-7109, 2025.

[24] M. Chitour, S. Benguediab, A. Bouhadra, F. Bourada, M. Benguediab, A. Tounsi, Effect of variable volume fraction distribution and geometrical parameters on the bending behavior of sandwich plates with FG isotropic face sheets, *Mechanics Based Design of Structures and Machines,* Vol. 52, No. 6, pp. 3079-3105, 2024.

[25] W. Fang, T. Yu, T. Q. Bui, Analysis of thick porous beams by a quasi-3D theory and isogeometric analysis, *Composite Structures,* Vol. 221, pp. 110890, 2019.

[26] K. Gao, R. Li, J. Yang, Dynamic characteristics of functionally graded porous beams with interval material properties, *Engineering Structures,* Vol. 197, pp. 109441, 2019.

[27] D. Chen, J. Yang, S. Kitipornchai, Elastic buckling and static bending of shear deformable functionally graded porous beam, *Composite Structures,* Vol. 133, pp. 54-61, 2015.

[28] N.-D. Nguyen, T.-N. Nguyen, T.-K. Nguyen, T. P. Vo, A new two-variable shear deformation theory for bending, free vibration and buckling analysis of functionally graded porous beams, *Composite Structures,* Vol. 282, pp. 115095, 2022.

[29] C. Mourad, B. Rebai, K. Mansouri, F. Khadraoui, A. Berkia, T. Messas, Investigating the influence of material composition on bending analysis of functionally graded beams using a 2D refined theory, *Journal of Computational Applied Mechanics,* Vol. 55, No. 1, pp. 62-76, 2024.

[30] N. Himeur, A. Menasria, A. Bouhadra, C. Mourad, S. Refrafi, L. Guessoum, A. Ouchene, S. Lebouazda, Buckling and bending analysis of porous FG beam using a simple integral quasi-3D theory, *Journal of Applied Mathematics and Computational Mechanics,* Vol. 23, No. 4, pp. 30-41, 2024.

[31] Y. Lee, X. Zhao, K. M. Liew, Thermoelastic analysis of functionally graded plates using the element-free kp-Ritz method, *Smart Materials and Structures,* Vol. 18, No. 3, pp. 035007, 2009.

[32] Q.-H. Pham, P.-C. Nguyen, V. K. Tran, T. Nguyen-Thoi, Isogeometric analysis for free vibration of bidirectional functionally graded plates in the fluid medium, *Defence Technology,* Vol. 18, No. 8, pp. 1311-1329, 2022.

[33] A. Menasria, R. Slimani, A. Bouhadra, S. Refrafi, M. Chitour, M. A. Rachedi, N. Himeur, K. Zerari, A simple quasi-3D theory for static stability analysis of imperfect FG beam, *Archives of Mechanics,* Vol. 77, No. 3, pp. 263-287, 2025.

[34] B. M. Shinde, A. S. Sayyad, A new higher order shear and normal deformation theory for FGM sandwich shells, *Composite Structures,* Vol. 280, pp. 114865, 2022.

[35] A. S. Sayyad, Y. M. Ghugal, T. Kant, Higher-order static and free vibration analysis of doubly-curved FGM sandwich shallow shells, *Forces in Mechanics,* Vol. 11, pp. 100194, 2023.

[36] S. Benounas, M.-O. Belarbi, V. P. Van, A. A. Daikh, Precise analysis of the static bending response of functionally graded doubly curved shallow shells via an improved finite element shear model, *Engineering Structures,* Vol. 319, pp. 118829, 2024.

[37] X. Zhao, Y. Lee, K. M. Liew, Thermoelastic and vibration analysis of functionally graded cylindrical shells, *International Journal of Mechanical Sciences,* Vol. 51, No. 9-10, pp. 694-707, 2009.

[38] E. Viola, L. Rossetti, N. Fantuzzi, Numerical investigation of functionally graded cylindrical shells and panels using the generalized unconstrained third order theory coupled with the stress recovery, *Composite Structures,* Vol. 94, No. 12, pp. 3736-3758, 2012.

[39] A. A. Belhachemi, D. Ouinas, M. R. Ghezzar, F. Zohra Zaoui, B. Achour, M. S. A. Houari, J. A. Viña Olay, Assessment of new four variables 2D and quasi-3D higher order shear theories for bending analysis of different double curved FG shells, *Mechanics of Advanced Materials and Structures,* Vol. 32, No. 10, pp. 2181-2201, 2025.